Surface steps dominate the water formation on Pd(111) surfaces

(article starts on next page)

Surface steps dominate the water formation on Pd(111) surfaces

Elisabeth M. Dietze, Lin Chen and Henrik Grönbeck

View Online   Export Citation   CrossMark

ARTICLES YOU MAY BE INTERESTED IN

Surface steps dominate the water formation on Pd(111) surfaces

View Online   Export Citation   CrossMark

Elisabeth M. Dietze,[a] 🆔 Lin Chen, 🆔 and Henrik Grönbeck[b] 🆔

AFFILIATIONS

Department of Physics and Competence Centre for Catalysis, Chalmers University of Technology, Göteborg, Sweden

[a]Author to whom correspondence should be addressed: dietze@chalmers.se
[b]E-mail: ghj@chalmers.se

ABSTRACT

Water formation is relevant in many technological processes and is also an important model reaction. Although water formation over Pd surfaces is widely studied, questions regarding the active site and the main reaction path ($OH^* + OH^*$) or ($OH^* + H^*$) are still open. Combining first-principles density functional theory calculations and kinetic Monte Carlo simulations, we find that the reaction rate is dominated by surface steps and point defects over a wide range of conditions. The main reaction path is found to be temperature dependent where the $OH^* + OH^*$ path dominates at low temperatures, whereas the $OH^* + H^*$ path is the main path at high temperatures. Steps facilitate the OH^* formation, which is the rate limiting step under all conditions. OH^* is formed via $O^* + H^*$ association or OOH^* splitting at low temperatures, whereas OH^* is exclusively formed via $O^* + H^*$ association at high temperatures. The results of the first-principles-based kinetic model are in excellent agreement with experimental observations at high and low temperatures as well as different gas-phase compositions.

INTRODUCTION

Water is a simple molecule and one of the most abundant compounds on earth. Water is, furthermore, relevant in a range of technological applications. Water splitting ($H_2O \rightarrow H_2 + 1/2O_2$) and the water–gas-shift reaction ($H_2O + CO \rightarrow H_2 + CO_2$) are two examples of possible routes to use H_2O to obtain hydrogen, which is important in a fossil free society.[1,2] Another example is the formation of water from H_2 and O_2 in proton-exchange membrane fuel cells, which is a promising technology in a hydrogen-based energy system.[3,4] Moreover, also in reactions where water is not a reactant or product, the presence of water can influence the overall reaction paths[5,6] and thereby change the reaction dynamics and selectivity.[7] The central role of water for sustainable energy systems is one reason to develop detailed knowledge on catalytic splitting and formation of water over solid surfaces. Another reason is to develop general concepts and understanding by studying a model reaction with a limited number of reaction steps. The understanding of active sites and dominant formation paths is important when making conclusions on selectivity.

Palladium is widely used in heterogeneous catalysis to catalyze oxidation[8–13] and hydrogenation reactions.[14–20] Water formation

from O_2 and H_2 over Pd surfaces has been studied extensively in the past (see, e.g., Refs. 21–25). Water is known to form readily over Pd via a Langmuir–Hinshelwood reaction. O_2 and H_2 dissociate into H and O after which OH is formed. H_2O is formed via either OH + OH or OH + H although the main path has been difficult to reveal experimentally.[22] OH formation has been identified as the rate limiting step and surface science experiments at low temperatures and pressures over Pd(111) have shown that OH is formed mainly over surface defects such as monoatomic steps.[23]

A detailed understanding of water formation from O_2 and H_2 over Pd has recently become important in connection to direct H_2O_2 formation over palladium nanoparticles.[26–31] A high selectivity to H_2O_2 requires that water formation is suppressed. Thus, it is imperative to know which sites and reaction paths facilitate water formation. Here, we present a combined density functional theory (DFT) and kinetic Monte Carlo (kMC) study to investigate water formation on metallic Pd(111) and stepped Pd surfaces over a wide range of temperature and pressure conditions. The model includes multiple paths to both H_2O and H_2O_2. The kMC model is validated by comparison with surface science experiments at low temperatures[23] and experiments on a polycrystalline Pd foil at high temperatures.[24] We conclude that steps control the catalytic

activity and that the main path for water formation is temperature dependent.

COMPUTATIONAL METHODS

First-principles calculations

Density functional theory (DFT) as implemented in VASP[32–34] is used to obtain adsorption and reaction energies for various species derived from H_2 and O_2 adsorption on Pd(111) and Pd(211) surfaces, respectively.[30] The employed surface structures are shown in Figs. S1–S3 of the supplementary material.

All calculations are done with the Perdew–Burke–Ernzerhof (PBE)[35] functional augmented with the dispersion correction D3 proposed by Grimme et al.[36,37] The plane augmented wave method[38,39] is used to describe the interactions between ionic cores and valence electrons, and a cut-off energy of 450 eV is chosen for the plane-wave expansion. A $(4 \times 4 \times 1)$ k-point density is used to sample the Brillouin zone using a Monkhorst–Pack scheme.[40] Total energies are in the self-consistent cycle converged to 10^{-5} eV, and structures are considered to be converged if the largest force in the system is lower than 0.03 eV/Å. The bulk lattice constant for Pd is optimized to be 3.89 Å. The employed surface cells are $p(3 \times 3)$ and $p(1 \times 2)$ for Pd(111) and Pd(211), respectively, and consist of four layers of which the two bottom layers are frozen to the bulk lattice. The slabs are separated by 12 Å of vacuum.

Nudge elastic band (NEB) calculations are used to find the transition states as implemented in the transition state tools for VASP by Henkelman and co-workers.[41,42] Vibrational modes are calculated using finite differences and fixing all surface metal atoms. Transition states have one imaginary frequency along the reaction coordinate. The vibrations are also used to calculate zero-point energy corrections and entropy contributions to the free energy. The vibrational energies are reported in Tables S2 and S3 of the supplementary material.

Reaction scheme

Figure 1 shows the reaction scheme for water formation on Pd surfaces. To obtain a closed reaction cycle, two H_2O molecules are formed from one O_2 and two H_2. The network also contains the possibility of H_2O_2 formation.

The first step in the cycle is molecular hydrogen adsorption and instantaneous dissociation into H^*. Molecular oxygen is instead adsorbed into a molecular precursor state $O_2{}^*$. From the precursor state, $O_2{}^*$ can be either directly hydroxylated to OOH^*, entering the H_2O_2 cycle, or dissociated into O^*. OH^* is formed from atomic hydrogen and oxygen. OH^* may also be formed by OOH^* splitting into $OH^* + O^*$ or $H_2O_2{}^*$ splitting into $2OH^*$, which are the connections between the H_2O_2- and water-cycles. Water can be formed by either $OH^* + H^*$ or $OH^* + OH^*$ and desorbs when formed from the Pd surface. In the cycle, the second hydrogen molecule adsorbs dissociatively and OH^* is formed from $O^* + H^*$ and H_2O from $OH^* + H^*$. The surface has a coverage of intermediates during operating conditions, and the actual path for H_2O formation may depend on the conditions.

Figures 2(a) and 2(b) show the potential energy surfaces for the reaction cycles in Fig. 1 over Pd(111) and Pd(211), respectively. The numerical values are reported in Table S1 of the supplementary
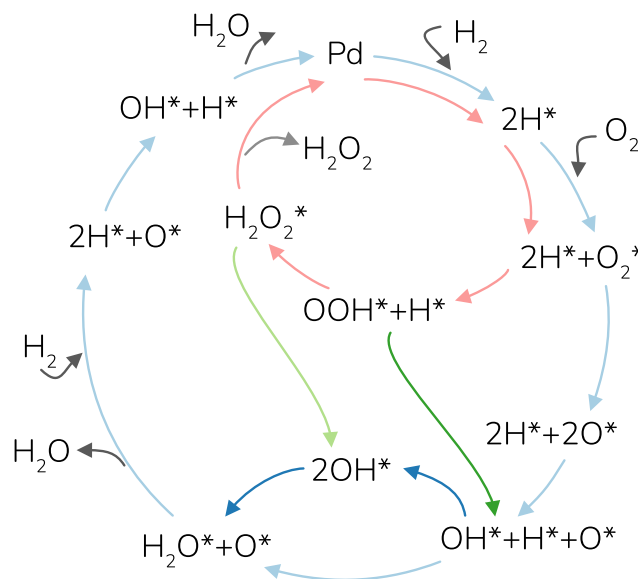

FIG. 1. Reaction network of water formation (light blue) with the dark blue arrows highlighting the water formation path via $OH^* + OH^*$. The cycle for H_2O_2 formation is shown in pink. The H_2O_2 cycle is connected to the water cycle via the splitting of OOH^* to O^* and OH^* (light green) and the splitting of $H_2O_2{}^*$ to $2OH^*$ (dark green).

material. The reaction energy to form water from H_2 and 0.5 O_2 is calculated to be 2.52 eV, which is close to the experimental value of 2.50 eV. The adsorption energy of O^* with respect to O_2 in the gas phase on both surfaces is about −1.4 eV. The slight difference between the final states in the potential energy landscapes for the two surfaces is due to differences in adsorbate–adsorbate interactions along the reaction path. The coverage of O^* is low in the modeled catalytic cycles, whereas the hydrogen coverage is sizable at high H_2 pressures. Key steps are therefore considered with a hydrogen coverage to effectively account for adsorbate–adsorbate interactions in the model.

The exothermicity of O_2 adsorption and H_2 splitting is similar for the two surfaces. The formation of H_2O_2 is endothermic over Pd(111), whereas the OOH^* formation over Pd(211) is exothermic. The process of OO-scission in OOH^* and $H_2O_2{}^*$ is exothermic and connected with low barriers on both surfaces. The barrier for the dissociation of O_2 from the adsorbed state ($O_2{}^*$) is higher than the barrier for OOH^* formation on both surfaces.

Considering H_2O formation over Pd(111), OH^* formation from O^*+H^* is associated with a barrier of 0.98 eV, which is clearly higher than the barrier for $O_2{}^*$ dissociation being 0.64 eV. The situation for H_2O formation is different on Pd(211), where the barrier for OH^* formation from $O^* + H^*$ is comparable with that of $O_2{}^*$ dissociation. The formation of H_2O^* from $OH^* + H^*$ has a higher barrier than H_2O formation from $OH^* + OH^*$.

H_2 does not adsorb along the step-edge and is therefore modeled only over (111)-sites. In the case of O_2 dissociation on the step-edge, the oxygen atoms are transferred directly to the terrace sites. As H^* and O^* are adsorbed preferably on terrace sites, reactions at steps require O^* and H^* from the terrace.
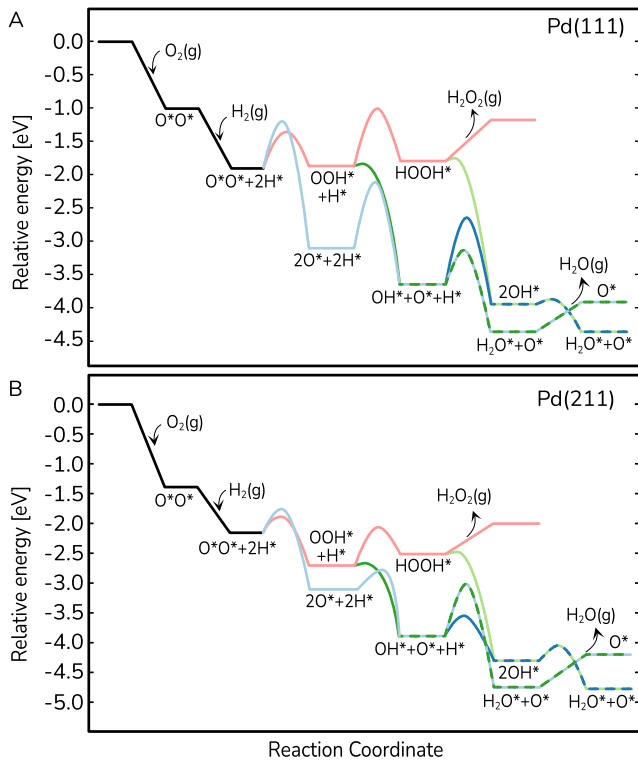
FIG. 2. Potential energy profiles for H_2O formation from H_2 and O_2 over (a) Pd(111) and (b) Pd(211). The blue paths show the water formation from $2H^* + 2O^*$, whereas the green paths show the additional water formation possibilities after entering the H_2O_2 formation path. The pink path shows the formation of H_2O_2. The H_2 dissociation for the Pd(211) profile is considered over the adjacent (111) sites.

Kinetic Monte Carlo model

The applied kinetic Monte Carlo model is based on Monte-Coffee.[43] The adsorption rates are obtained from collision theory,

$$k_{ads}^+ = \frac{p \cdot S_0 \cdot A}{\sqrt{2 \cdot \pi \cdot m \cdot k_B T}}, \qquad (1)$$

with p being the partial pressure, S_0 being the sticking coefficient, A being the surface site area, m being the mass, k_B being Boltzmann's constant, and T being the temperature. The corresponding desorption rates are calculated assuming equilibrium between adsorption and desorption,

$$K_{eq} = k^+/k^- = e^{\frac{\Delta S^\ddagger}{k_B}} \cdot e^{-\frac{\Delta E}{k_B T}}, \qquad (2)$$

with k^+ and k^- being the forward and backward reaction rate, respectively. $\Delta S^\ddagger$ is the change in entropy, and ΔE is the change in energy, omitting the pV-term in the Gibbs free energy. The rates of reactions are calculated from transition state theory,

$$k_{\beta\alpha}^+ = \frac{k_B \cdot T}{h} e^{\frac{\Delta S}{k_B}} \cdot e^{-\frac{E_a}{k_B T}}. \qquad (3)$$

E_a is the reaction barrier.

All reactions as shown in Fig. 1 are taken into account in the kinetic model. Thus, each arrow in Fig. 1 is defined as one event in the kinetic model augmented with the corresponding events for the backward reactions. Additionally, the diffusion of the surface species (H^*, O^*, O_2^*, OH^*, OOH^* and H_2O^*) are included. The diffusion rates are chosen to be fast in comparison to the other reactions.

The time $t_{\beta\alpha}$ to advance the system from the current state α to the future state β is calculated for all possible processes. Following the first reaction method,[44] the event is executed, which has the lowest $t_{\beta\alpha}$. The time is advanced according to $t \rightarrow t + t_{\beta\alpha}$ with

$$t_{\beta\alpha} = 1 - \frac{1}{k_{\beta\alpha}} \cdot \ln \rho, \qquad (4)$$

where ρ is a random number between 0 and 1 and $k_{\beta\alpha}$ is the rate for the transition from state α to β. We assume that the executed event affects the system state locally and, therefore, only evaluate new times for events close to the last active site. The local updating reduces the number of time evaluations, which is usually the bottleneck for the first reaction method.[45]

The surface is modeled using periodic boundary conditions with a (40×20) (111) super-cell consisting of 800 sites [Fig. 3(a)]. Each site is connected to six nearest neighbors [Fig. 3(b)]. Sites on a surface form geometric sites such as atop, hollow, and bridge. Here, we employ a coarse-grained site scheme in which each species occupies a geometrical site although the character of the geometric site is not treated explicitly. Each event is connected to a unique nearest-neighbor site pair.
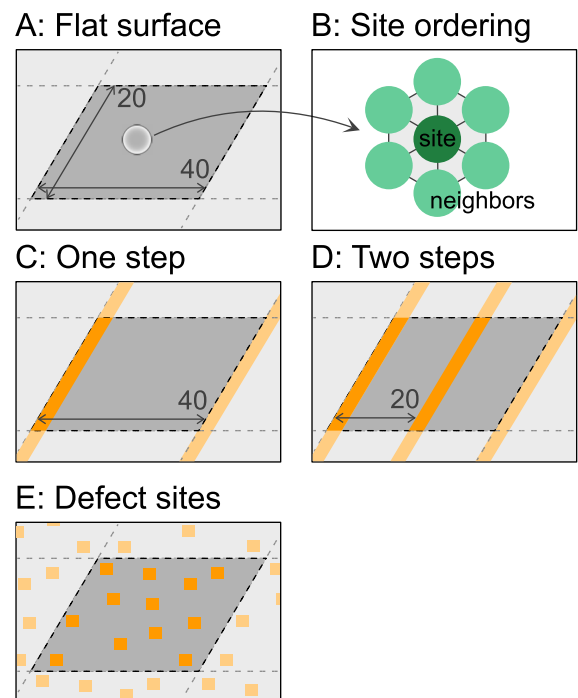
FIG. 3. Schematic of the model systems. (a) (40×20) super-cell of a pristine Pd(111) surface, (b) site connectivity, (c) Pd(111) with one step, (d) Pd(111) with two steps, and (e) Pd(111) with 5% homogeneously distributed defect sites.

Simulations are performed for pristine (111) surfaces, stepped (111) surfaces, and surfaces with point defects. Stepped surfaces are represented by replacing one row of terrace sites parallel to the lattice direction, with step sites (20 sites = 2.5%), as illustrated in Fig. 3(c). A higher step density is modeled by adding a second row in the center of the terrace [Fig. 3(d)]. The number of step sites increases to 5% with two steps. The potential landscape of Pd(211) is used to model the step sites. To model a situation where defect sites are homogeneously distributed, we also considered a surface with 5% of point defects [see Fig. 3(e)]. To allow for a direct comparison to the results for the stepped surfaces, the defect sites are given the same reaction properties as the step sites.

The turn-over frequency (TOF) for H_2O is calculated as the number of desorbed H_2O molecules from the surface divided by the total number of surface sites and simulation run-time,

$$TOF(H_2O) = \frac{N_{form}^{H_2O}}{N_{sites} \cdot t_{kMC}}. \quad (5)$$

Contributions to the $TOF(H_2O)$ from the $OH^* + H^*$ and $OH^* + OH^*$ paths, respectively, are calculated from

$$TOF = \frac{N_{form}^{Path}}{N_{sites} \cdot t_{kMC}}. \quad (6)$$

No dissociation or adsorption of H_2O is observed in any simulation.

KINETIC SIMULATIONS

The explored reaction network is general and describes H_2 oxidation at different conditions. We study the reaction at low and high temperatures as well as different gas-phase pressures and compositions. We start the discussion with the low temperature results where the detailed surface science experiments with well characterized surfaces by Mitsui et al.[23,46] allow for a straight-forward comparison and validation of the computational approach.

Low temperature reaction mechanism

Mitsui et al.[23,46] studied H_2 oxidation over a stepped Pd(111) surface with Scanning Tunneling Microscopy (STM). The reaction was performed by exposing an oxygen precovered surface to a low pressure of hydrogen ($p_{H_2} = 1.3 \times 10^{-5}$ Pa). Water formation was measured at temperatures above 220 K as a depletion of the oxygen coverage after 20 min hydrogen exposure. Similar onset temperatures for water formation over Pd(111) were observed by Pauer and Winkler[47] for comparable pressures of H_2 and O_2.

Here, we consider three different surfaces to compare with the surface science experiments,[23] namely, a pristine Pd(111) surface, Pd(111) with one step, and Pd(111) with two steps. Following the experiments, the surfaces are precovered with oxygen forming a 2×2 structure. The oxygen precovered surfaces are exposed to a hydrogen pressure of $p_{H_2} = 1.3 \times 10^{-5}$ Pa, whereas all other pressures (p_{O_2,H_2O,H_2O_2}) are set to 10^{-30} Pa. The kMC simulation is terminated if either all adsorbed oxygen atoms are transformed into water or $t_{sim} \geq 30$ min.

Figure 4 shows the number of formed H_2O molecules as a function of temperature. For the pristine Pd(111) surface, no formation
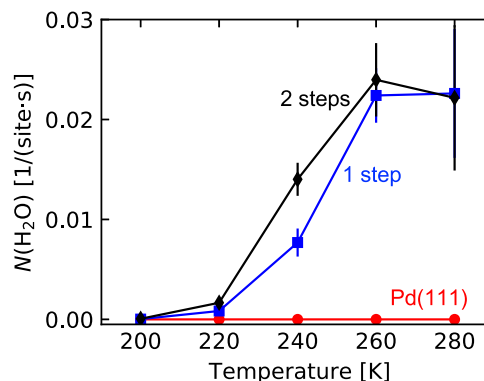

FIG. 4. Temperature dependent number of formed water molecules over Pd(111) (red), one step (blue), and two steps (black) per site over a precovered oxygen surface. $p_{H_2} = 1.3 \cdot 10^{-5}$ Pa.

of H_2O is observed. Water is instead formed over the stepped surfaces. The calculated onset temperature for H_2O formation is about 220 K, which is in good agreement with the experiments.[23] The rate of the reaction is also in good agreement with the experiments, as shown in the Appendix.

Analyzing the path for water formation, OH^* can only form via $O^* + H^*$ under these conditions. We find that OH^* is preferably formed at the steps, which is linked to the lower barrier for OH^* formation on these sites (see Table S1 of the supplementary material. Because of the stronger adsorption energy of OH^* on the step as compared to the Pd(111) terrace, OH^* accumulates and diffuses along the step and H_2O is formed via the $OH^* + OH^*$ pathway. The preferred reaction path agrees with the interpretation of the STM measurements in Ref. 23.

Partial pressure dependence

Having established the computational approach by the detailed comparison with surface science experiments, we turn to the complete water formation cycle, which includes O_2 adsorption from the gas phase. In this part, we are comparing the influence of total pressure p_{tot} and partial pressure of hydrogen and oxygen on the H_2O formation at 300 K. The simulations are performed as a function of the relative hydrogen concentration α_{H_2},

$$\alpha_{H_2} = \frac{p_{H_2}}{p_{H_2} + p_{O_2}}. \quad (7)$$

We chose $\alpha_{H_2} = 0.1, 0.5, 0.9$ to investigate conditions with hydrogen deficiency and excess, respectively. The total pressures are chosen to be $p_{tot} = 10^{-5}, 10^{-4}$, and 10^{-3} Pa, respectively. The pressures are chosen to avoid both Pd oxide and hydride formation.[30] For each set of parameters, we run 32 independent kMC simulations, initialized with an empty surface. Statistics are collected after an equilibration period of 10^5 kMC steps. In the following, we discuss OH^* and H_2O formation focusing on the surface with two steps. A similar discussion is presented in Fig. S4 for the pristine surface in the supplementary material.

Because OH^* formation is rate limiting, we analyze in Fig. 5(a) the contribution of the two paths for OH^* formation. OH^* can
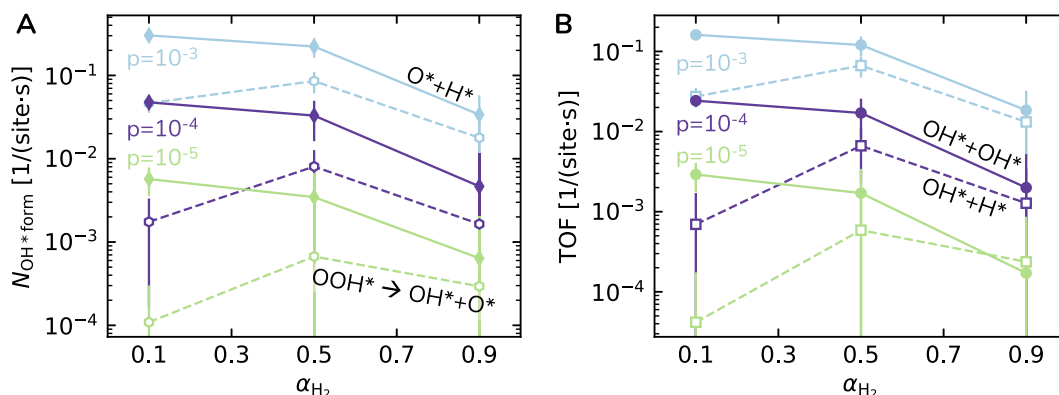
FIG. 5. Water formation over a stepped Pd(111) surface (5% step sites). (a) Contributions to the OH* formation via the O* + H* (solid lines) and OOH* splitting paths (dashed lines). (b) Contributions to water formation via the OH* + OH* (solid lines) and OH* + H* paths (dashed lines). Reaction conditions are T = 300 K and total pressures of p_{tot} = 10^{-3}, 10^{-4}, and 10^{-5} Pa, respectively (light blue, violet, and green) for different p_{H_2} : p_{O_2} ratios.

under the simulated conditions be formed either by O* + H* association or by OOH* dissociation into OH* + O*. The O* + H* path is dominating for all pressures and α_{H_2} values. At H_2 deficient conditions, the contribution from the O* + H* path is about one magnitude larger than the OOH* path. The difference reduces as the H_2 concentration increases, which is an effect of competition between O_2^* dissociation and OOH* formation. The overall OH* formation is largest for 10^{-3} Pa and lowest for 10^{-5} Pa. Although OOH* is formed, we do not observe H_2O_2 formation, which is in agreement with previous mean-field simulations over Pd(111).[30] The coverages for the total pressure of 10^{-3} Pa are reported in Fig. S3. The surface coverage is dominated by either O* or H* depending on α_{H_2}. The total coverage is at all mixtures below 55%.

The water formation is shown in Fig. 5(b). Water is formed by either OH* + OH* or OH* + H*. For low α_{H_2} values (hydrogen deficiency), the OH* + OH* path is dominating. However, the importance of the OH* + H* path increases with increasing hydrogen concentration. The reason for the larger OH* + H* contribution in hydrogen excess is that the probability of adsorbed OH* at the step close to a neighboring H* at the terrace increases with H* coverage. Higher total gas-phase pressures result in higher H_2O formation rates.

Comparing the results for OH* and H_2O formation, we notice that the H_2O formation from OH* + OH* closely follows the OH* formation from O* + H*. This is the consequence of that OH*

TABLE I. Experimentally measured apparent activation energies for OH formation in eV and prefactors in s^{-1}.

E_a	A	References
0.62	10^{10}	Measured over a polycrystalline Pd foil[24]
0.62–0.82	10^{10}–10^{13}	Measured on a Pd-MOS device[22]
0.3	6×10^7	Molecular beam study over Pd(111)[21]
≤0.42		Oxygen precovered stepped Pd surface[23]

formation is the rate limiting step and preferentially formed at steps. The barrier for O* + H* is 0.26 eV at the step, whereas the barrier for OH* + OH* is 0.24 eV. Experimentally, apparent activation energies and prefactors for OH* formation have been measured and some examples are given in Table I. The apparent activation energies vary in the range of 0.3–0.82 eV, and the prefactors vary between 10^7 and 10^{13}. Generally, a low apparent activation energy is combined with a low prefactor. At 300 K, our calculated prefactors for O* + H* are 8×10^{12} for (111) and 6×10^{12} for the step, respectively. As the prefactor is determined by the vibrational partition functions, they are similar despite very different reaction barriers, which are 0.98 eV for Pd(111) and 0.26 eV for Pd(211).
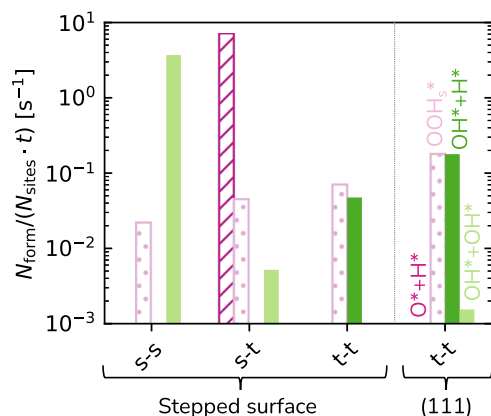
The simulations reveal a possible reason for the large range of apparent activation energies reported in the literature.[21–24] The simulations show that two paths contribute to OH* formation and that the relative importance changes with reaction conditions.

After elucidating the main reaction paths, we are analyzing the contributions from the different types of sites. In Fig. 6, we show the site contributions for OH* and the H_2O formation, respectively. The results for the other H_2 concentrations are presented in Fig. S5 of the supplementary material. In general, the O* + H* and OH* + H* paths have only two possible site combinations: step–terrace and terrace–terrace, respectively. The step–step combination does not occur as H* does not bind on the step but to terrace sites adjacent to step sites. The step–step combination is possible for the OOH* dissociation and OH* + OH* water formation.

Over the pristine surface, OH* is formed exclusively via OOH* dissociation to OH* + O*. H_2O is formed mainly from OH* + H* with some contributions from OH* + OH*. At the stepped surface, OH* formation via OOH* dissociation occurs at all site combinations. OH* formation from O* + H* is, instead, exclusively taking place at step–terrace sites. H_2O is dominantly formed at the step from OH* + OH*. For the surface with steps, the OH* + H* path at the terrace sites contributes similarly to the H_2O formation as over the pristine Pd(111) surface. The results highlight the importance of steps in the H_2O formation and show how the presence of different sites opens alternative reaction paths.

FIG. 6. Number of formed OH* and H_2O molecules per site type on Pd(111) with two steps (left) and pristine Pd(111) (right). Dark, striped pink: $O^* + H^*$, dotted pink: OOH* splitting, dark green: $OH^* + H^*$, and light green: $OH^* + OH^*$. The step and terrace sites are denoted as s and t, respectively. $T = 300$ K, $p_{tot} = 10^{-3}$ Pa, and $\alpha_{H_2} = 0.1$.

High temperature

To evaluate how the main reaction mechanism depends on reaction conditions, we also consider water formation at high temperature and medium pressure. The reaction conditions are chosen to compare with the experiments of Johansson et al.[24] where the reaction was studied at a total pressure of 26 Pa and a temperature of 1300 K. The reaction was studied over a polycrystalline Pd foil by Laser Induced Fluorescence (LIF) and microcalorimetry in Ref. [24]. Here, we simulate the reaction using the same surface cell size as for the low temperature cases and the double stepped surface. Additionally, we also investigate the case of 5% defect sites. The high temperature probably leads to a continuous reconstruction of the surface in the experiments. Although the simulations do not account explicitly for the surface dynamics, the presence of different types of sites effectively models a rough surface.

The dissociation of adsorbed O_2^* is very fast at 1300 K, which implies that molecular oxygen is not present on the surface. Thus, OOH* and subsequent H_2O_2 formation can be neglected, and we have therefore omitted reactions 4–7 and 11 (see Table S1 of the supplementary material) in the high-temperature simulations. The validation of this assumption is shown in Fig. S7 of the supplementary material. In Ref. [24], OH radicals were measured in the gas phase over the foil at low α_{H_2}. We have not included these desorption and re-adsorption steps that appear at low α_{H_2}.

Figure 7(a) shows the TOF for the pristine surface (blue), the surface with two steps (orange), and a surface with 5% defective sites (green). The defective surface exhibits the highest TOF, and the pristine surface exhibits the lowest TOF. In all three cases, the TOF has a maximum at about $\alpha_{H_2} = 0.4$. The maximum is not at $\alpha_{H_2} = 0.5$, which emphasizes that the reaction is dominated by a reaction step requiring a $H_2:O_2 = 1:1$ ratio (the OH* formation) rather than reaction steps with a 2:1 stoichiometry.[24] To compare directly to the experiments of Johansson et al.,[24] we include the experimental results from Fig. 4[24] measured at 200 SCCM. The simulated results for both the stepped and defective surfaces show very
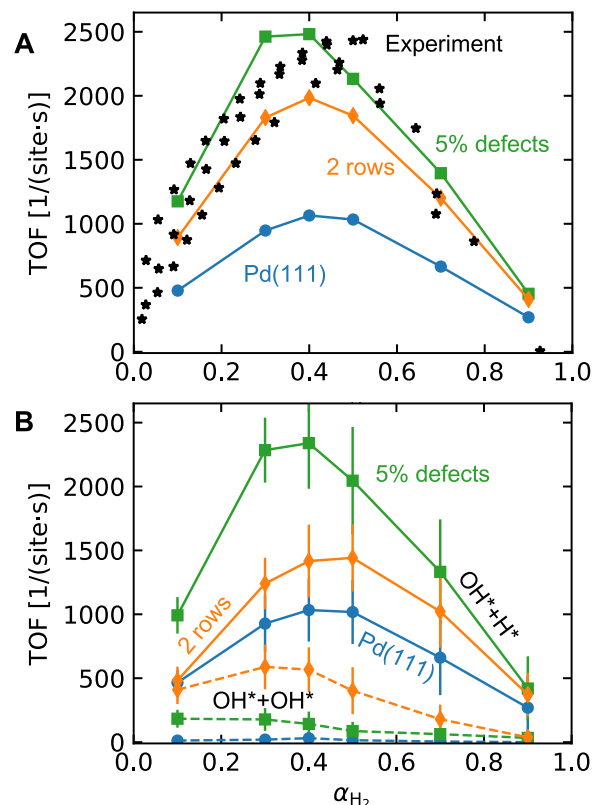

FIG. 7. (a) Total water turn-over frequency (TOF) for $T = 1300$ K and $p_{tot} = 26$ Pa and three different surfaces: blue: Pd(111), orange: Pd(111) with two steps and green: Pd(111) with 5% defect sites. (b) Contributions to the water formation from the $OH^* + H^*$ path (solid lines) and $OH^* + OH^*$ path (dashed lines) as shown in panel (a).

good quantitative agreement with the measurements within a 10% error margin.

To deconvolute the different contributions to the TOF, Fig. 7(b) shows the H_2O formation for the $OH^* + H^*$ and $OH^* + OH^*$ paths. The $OH^* + H^*$ path dominates for all surfaces, and the $OH^* + OH^*$ path is only relevant for the surface with two steps at α_{H_2} lower than 0.5. The $OH^* + OH^*$ path is relevant only at low α_{H_2} because of the low coverage of H^*.

The sites contribute uniquely to the water formation. The number of formed H_2O molecules per surface site types for the different possible site combinations is presented in Fig. 8. Note that the TOF in Fig. 8 is per surface site type, which means that the sum of the different contributions is not directly comparable with the value in Fig. 7. We find that, in general, α_{H_2} does not affect which sites dominate water formation. Over pristine Pd(111), we find that only the $OH^* + H^*$ reaction path contributes to water formation. OH^* is at high temperatures formed via $O^* + H^*$, which is in contrast to the low temperature case where OH^* is formed via OOH* dissociation. For the stepped and defective surfaces, H_2O is formed mainly over step sites. The surface with two steps is the only surface that has water formation from $OH^* + OH^*$, where both OH^* are adsorbed at step sites. This result shows that the presence of surface
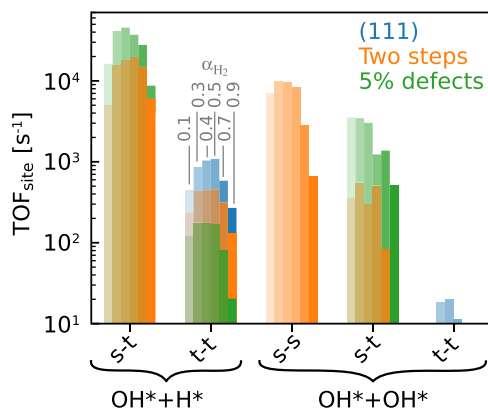
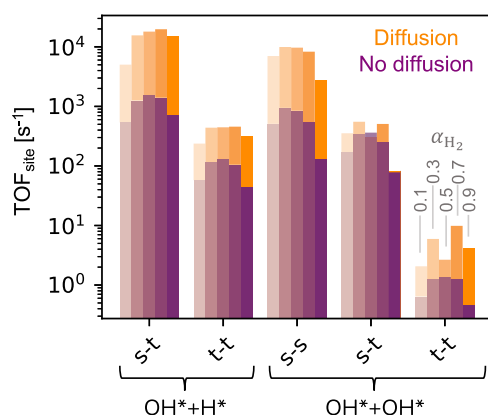**FIG. 8.** Turn-over frequency (TOF) per site type for T = 1300 K and p_{tot} = 26 Pa for the OH* + H* path and OH* + OH* path, respectively, and the involved surface sites. Step and terrace sites are denoted as s and t, respectively. The colored bars give the contributions for two surface steps per unit cell (orange), the (111) surface (blue), and 5% defect sites (green).

steps enhances the reaction by opening up a favorable reaction path. The contribution from the OH* + OH* path over step sites reduces as a function of hydrogen concentration as the hydrogen coverage increases. On the defective surface, the step–terrace sites dominate the water formation via the OH* + H* path. The contribution from water formation over only terrace sites (t–t) is small for the defective surfaces.

The site-specific contributions to the TOF show that reactions including different types of sites are important. Moreover, the diffusion of intermediates between different sites has a marked influence on the TOF. The influence of diffusion on the water formation reaction is analyzed in Fig. 9, which shows the number of formed H$_2$O molecules for the case with Pd(111) with two steps with (orange) and without (violet) diffusion for different α_{H_2}. The simulations without diffusion are performed by removing the diffusion events in the

reaction network. The comparison shows that the diffusion has a major impact on the overall number of formed water molecules as the TOF is increased by one order of magnitude including diffusion. The importance of the diffusion is present for all gas-phase compositions, and both the OH* + H* and OH* + OH* reactions are affected.

CONCLUSIONS

Using a first-principles-based kinetic Monte Carlo approach, we have investigated water formation from H$_2$ and O$_2$ over metallic Pd surfaces including reaction paths that are relevant for both H$_2$O and H$_2$O$_2$ formation. The reaction has been studied over pristine Pd(111) as well as surfaces with steps or defects at low and high temperatures and different gas-phase compositions. The simulated TOFs agree quantitatively with previous experiments for both low and high temperature conditions.

We find that surface steps dominate H$_2$O formation and that pristine Pd(111) is inactive at low temperatures. The mere presence of sites with step-like properties enhances the activity as homogeneously distributed point defects yield a TOF that is similar to a stepped surface. The main reaction path changes with temperature and gas-phase composition. At low temperatures, OH* formation proceeds through either OOH* dissociation or O* + H* association. H$_2$O is formed subsequently through both the OH* + OH* and the OH* + H path. At high temperatures, OH* is exclusively formed through O* + H* association, whereas both reaction paths for water formation (OH* + OH* and OH* + H) contribute to the TOF. We find that the possibility of diffusion between the different types of sites enhances the activity.

The present work demonstrates the robustness of first-principles-based kinetic models with atomistic resolution. In general, detailed understanding of dominant reaction paths and identification of active sites is crucial to analyze experimental activity and selectivity and provides guidelines to increase the performance of existing catalysts.

SUPPLEMENTARY MATERIAL

See the supplementary material for reaction energies and barriers, considered structures in the DFT calculations, reaction path contributions to OH* and water formation at low temperatures, pressure and reactant composition effects on site contributions at low temperatures, surface coverages at low temperatures, and reaction path contribution to OH* formation at high temperature.

FIG. 9. Turn-over frequency per site type for T = 1300 K and p_{tot} = 26 Pa for Pd(111) with two steps for the case when diffusion is allowed (orange) and for the case without diffusion (violet) for different α_{H_2O} (color brightness). Step and terrace sites are denoted as s and t, respectively.

AUTHOR DECLARATIONS

Conflict of Interest

The authors do not have any conflicts of interest.

DATA AVAILABILITY

The data that support the findings of this study are available within the article and its supplementary material.

APPENDIX: ANALYSIS OF EXPERIMENTAL RATES

Mitsui et al.[23] investigated two Pd(111) terraces separated by a monoatomic step. The surface was first exposed to O_2 at high enough temperatures to form a (2×2) oxygen overlayer. Using a STM, the initial surface area covered with oxygen (A_{init}) was measured to be 2130 and 900 nm^2 for the two terraces, respectively. After 20 min of hydrogen exposure, the final surface area covered with oxygen (A_{final}) was measured to be 1840 and 605 nm^2 for the two terraces, respectively. Given that the (2×2) structure contains four oxygen atoms and corresponds to an area of 0.26 nm^2 (A_{Pd2x2}), the number of adsorbed oxygen atoms can be calculated. Assuming that all reacted oxygen atoms (N_O^{react}) form water, the number of formed water molecules per second ($n_{H_2O}^{form}$) can be calculated,

$$N_O^{react} = \frac{A_{init} - A_{final}}{A_{Pd2x2}}, \tag{A1}$$

$$n_{H_2O}^{form} = \frac{N_O^{react}}{\Delta t}. \tag{A2}$$

Analyzing the STM data, $n_{H_2O}^{form}$ is calculated to be 0.92 and 0.94 1/s for the two terraces at 223 K. We calculate the number of reacted oxygen atoms per second and site from the pre-adsorbed oxygen atoms at 220 K to be 0.67 (0.66) 1/s for the surface with one (two) step.

REFERENCES

[1] I. Dincer and C. Acar, "Review and evaluation of hydrogen production methods for better sustainability," Int. J. Hydrogen Energy 40, 11094–11111 (2014).

[2] P. Nikolaidis and A. Poullikkas, "A comparative overview of hydrogen production processes," Renewable Sustainable Energy Rev. 67, 597–611 (2017).

[3] W. R. W. Daud, R. E. Rosli, E. H. Majlan, S. A. A. Hamid, R. Mohamed, and T. Husaini, "PEM fuel cell system control: A review," Renewable Energy 113, 620–638 (2017).

[4] Y. Wang, D. F. Ruiz Diaz, K. S. Chen, Z. Wang, and X. C. Adroher, "Materials, technological status, and fundamentals of PEM fuel cells—A review," Mater. Today 32, 178–203 (2020).

[5] J. Bergeld, B. Kasemo, and D. Chakarov, "CO oxidation on Pt(111) promoted by coadsorbed H_2O," Surf. Sci. 495, L815–L820 (2001).

[6] K. B. Sravan Kumar, T. N. Whittaker, C. Peterson, L. C. Grabow, and B. D. Chandler, "Water poisons H_2 activation at the Au-TiO_2 interface by slowing proton and electron transfer between Au and titania," J. Am. Chem. Soc. 142, 5760–5772 (2020).

[7] J. Saavedra, T. Whittaker, Z. Chen, C. J. Pursell, R. M. Rioux, and B. D. Chandler, "Controlling activity and selectivity using water in the Au-catalysed preferential oxidation of CO in H_2," Nat. Chem. 8, 584–589 (2016).

[8] A. D. Mayernick and M. J. Janik, "Methane oxidation on Pd-ceria: A DFT study of the mechanism over $Pd_xCe_{1-x}O_2$, Pd, and PdO," J. Catal. 278, 16–25 (2011).

[9] A. Hellman, A. Resta, N. M. Martin, J. Gustafson, A. Trinchero, P.-A. Carlsson, O. Balmes, R. Felici, R. van Rijn, J. W. M. Frenken, J. N. Andersen, E. Lundgren, and H. Grönbeck, "The active phase of palladium during methane oxidation," J. Phys. Chem. Lett. 3, 678–682 (2012).

[10] A. Trinchero, A. Hellman, and H. Grönbeck, "Methane oxidation over Pd and Pt studied by DFT and kinetic modeling," Surf. Sci. 616, 206–213 (2013).

[11] N. M. Martin, M. Van den Bossche, H. Grönbeck, C. Hakanoglu, F. Zhang, T. Li, J. Gustafson, J. F. Weaver, and E. Lundgren, "CO adsorption on clean and oxidized Pd(111)," J. Phys. Chem. C 118, 1118–1128 (2014).

[12] V. Bratan, C. Munteanu, C. Hornoiu, A. Vasile, F. Papa, R. State, S. Preda, D. Culita, and N. Ionescu, "CO oxidation over Pd supported catalysts—In situ study of the electric and catalytic properties," Appl. Catal. B: Environ. 207, 166–173 (2017).

[13] M. Monai, T. Montini, R. J. Gorte, and P. Fornasiero, "Catalytic oxidation of methane: Pd and beyond," Eur. J. Inorg. Chem. 2018, 2884–2893.

[14] O. Beeck, "Hydrogenation catalysts," Discuss. Faraday Soc. 8, 118–128 (1950).

[15] D. Stacchiola, S. Azad, L. Burkholder, and W. T. Tysoe, "An investigation of the reaction pathway for ethylene hydrogenations on Pd(111)," J. Phys. Chem. B 105, 11233–11239 (2001).

[16] D. Teschner, E. Vass, M. Hävecker, S. Zafeiratos, P. Schnörch, H. Sauer, A. Knopgericke, R. Schlögl, M. Chamam, A. Wootsch, A. S. Canning, J. J. Gamman, S. D. Jackson, J. McGregor, and L. F. Gladden, "Alkyne hydrogenation over Pd catalysts: A new paradigm," J. Catal. 242, 26–37 (2006).

[17] O. M. Wilson, M. R. Knecht, J. C. Garcia-Martinez, and R. M. Crooks, "Effect of Pd nanoparticle size on the catalytic hydrogenation of allyl alcohol," J. Am. Chem. Soc. 128, 4510–4511 (2006).

[18] C. J. Heard, C. Hu, M. Skoglundh, D. Creaser, and H. Grönbeck, "Kinetic regimes in ethylene hydrogenation over transition-metal surfaces," ACS Catal. 6, 3277–3286 (2016).

[19] A. Genest, J. Silvestre-Albero, W-Q. Li, N. Rösch, and G. Rupprechter, "The origin of the particle-size-dependent selectivity in 1-butene isomerization and hydrogenation on Pd/Al_2O_3 catalysts," Nat. Commun. 12, 6098 (2021).

[20] S. Cattaneo, S. Capelli, M. Stucchi, F. Bossola, V. Dal Santo, E. Araujo-Lopez, D. I. Sharapa, F. Studt, A. Villa, A. Chieregato, B. D. Vandegehuchte, and L. Prati, "Discovering the role of substrate in aldehyde hydrogenation," J. Catal. 399, 162–169 (2021).

[21] T. Engel and H. Kuipers, "A molecular-beam investigation of the reaction $H_2 + 12O_2 \rightarrow H_2O$ on Pd(111)," Surf. Sci. 90, 181–196 (1979).

[22] J. Fogelberg and L.-G. Petersson, "Kinetic modelling of the H_2–O_2 reaction on Pd and of its influence on the hydrogen response of a hydrogen sensitive Pd metal-oxide-semiconductor device," Surf. Sci. 350, 91–102 (1996).

[23] T. Mitsui, M. K. Rose, E. Fomin, D. F. Ogletree, and M. Salmeron, "A scanning tunneling microscopy study of the reaction between hydrogen and oxygen to form water on Pd(111)," J. Chem. Phys. 117, 5855–5858 (2002).

[24] Å. Johansson, M. Försth, and A. Rosén, "A comparative study of high-temperature water formation and OH desorption on polycrystalline palladium and platinum catalysts," Surf. Sci. 529, 247–266 (2003).

[25] M. Andersson and A. Rosén, "Adsorption and reactions of O_2 and D_2 on small free palladium clusters in a cluster-molecule scattering experiment," J. Phys.: Condens. Matter 22, 334223 (2010).

[26] C. H. Hyung, S. H. Gyeong, H. Jonghee, W. N. Suk, and H. L. Tae, "On the role of Pd ensembles in selective H_2O_2 formation on PdAu alloys," J. Phys. Chem. C 113, 12943–12945 (2009).

[27] N. M. Wilson and D. W. Flaherty, "Mechanism for the direct synthesis of H_2O_2 on Pd clusters: Heterolytic reaction pathways at the liquid-solid interface," J. Am. Chem. Soc. 138, 574–586 (2016).

[28] G. M. Lari, B. Puértolas, M. Shahrokhi, N. López, and J. Pérez-Ramírez, "Hybrid palladium nanoparticles for direct hydrogen peroxide synthesis: The key role of the ligand," Angew. Chem. 129, 1801–1805 (2017).

[29] X. Song, K. Sun, X. Hao, H.-Y. Su, X. Ma, and Y. Xu, "Facet-dependent of catalytic selectivity: The case of H_2O_2 direct synthesis on Pd surfaces," J. Phys. Chem. C 123, 26324–26337 (2019).

[30] L. Chen, J. W. Medlin, and H. Grönbeck, "On the reaction mechanism of direct H_2O_2 formation over Pd catalysts," ACS Catal. 11, 2735–2745 (2021).

[31] T. Ricciardulli, S. Gorthy, J. S. Adams, C. Thompson, A. M. Karim, M. Neurock, and D. W. Flaherty, "Effect of Pd coordination and isolation on the catalytic reduction of O_2 to H_2O_2 over PdAu bimetallic nanoparticles," J. Am. Chem. Soc. 143, 5445–5464 (2021).

[32] G. Kresse and J. Hafner, "Ab initio molecular dynamics for liquid metals," Phys. Rev. B 47, 558–561 (1993).

[33] G. Kresse and J. Hafner, "*Ab initio* molecular-dynamics simulation of the liquid-metal—Amorphous-semiconductor transition in germanium," Phys. Rev. B **49**, 14251–14269 (1994).

[34] G. Kresse and J. Furthmüller, "Efficient iterative schemes for *ab initio* total-energy calculations using a plane-wave basis set," Phys. Rev. B **54**, 11169–11186 (1996).

[35] J. P. Perdew, K. Burke, and M. Ernzerhof, "Generalized gradient approximation made simple," Phys. Rev. Lett. **78**, 1396 (1997).

[36] S. Grimme, J. Antony, S. Ehrlich, and H. Krieg, "A consistent and accurate *ab initio* parametrization of density functional dispersion correction (DFT-D) for the 94 elements H-Pu," J. Chem. Phys. **132**, 154104 (2010).

[37] S. Grimme, S. Ehrlich, and L. Goerigk, "Effect of the damping function in dispersion corrected density functional theory," J. Comput. Chem. **32**, 1456–1465 (2011).

[38] P. E. Blöchl, "Projector augmented-wave method," Phys. Rev. B **50**, 17953–17979 (1994).

[39] G. Kresse and D. Joubert, "From ultrasoft pseudopotentials to the projector augmented-wave method," Phys. Rev. B **59**, 1758–1775 (1999).

[40] H. J. Monkhorst and J. D. Pack, "Special points for Brillouin-zone integrations," Phys. Rev. B **13**, 5188–5192 (1976).

[41] G. Henkelman, B. P. Uberuaga, and H. Jónsson, "Climbing image nudged elastic band method for finding saddle points and minimum energy paths," J. Chem. Phys. **113**, 9901–9904 (2000).

[42] G. Henkelman and H. Jónsson, "Improved tangent estimate in the nudged elastic band method for finding minimum energy paths and saddle points," J. Chem. Phys. **113**, 9978–9985 (2000).

[43] M. Jørgensen and H. Grönbeck, "MonteCoffee: A programmable kinetic Monte Carlo framework," J. Chem. Phys. **149**, 114101 (2018).

[44] I. Mitrani, *Simulation Techniques for Discrete Event Systems* (Cambridge University Press, 1982), Vol. 14.

[45] A. P. J. Jansen, *An Introduction to Kinetic Monte Carlo Simulations of Surface Reactions* (Springer, Berlin, Heidelberg, 2012), pp. 37–71.

[46] T. Mitsui, M. K. Rose, E. Fomin, D. F. Ogletree, and M. Salmeron, "Coadsorption and interactions of O and H on Pd(111)," Surf. Sci. **511**, 259–266 (2002).

[47] G. Pauer and A. Winkler, "Water formation on Pd(111) by reaction of oxygen with atomic and molecular hydrogen," J. Chem. Phys. **120**, 3864–3870 (2004).